

1 **Surface energy dynamics and canopy structural properties in intact and disturbed** 2 **forests in the Southern Amazon**

3
4 Ekena Rangel Pinagé^{1,2}, David M. Bell³, Marcos Longo^{4,5}, Carlos A. Silva⁶, Ovidiu Csillik⁴,
5 Alfredo Huete¹

6 ¹ School of Life Sciences, University of Technology Sydney, Ultimo, NSW 2007, Australia. E-mail
7 address: alfredo.huete@uts.edu.au

8 ² College of Forestry, Oregon State University, Corvallis, OR 97333, USA. E-mail address:
9 rangelpe@oregonstate.edu

10 ³ Pacific Northwest Research Station, USDA Forest Service, Corvallis, OR 97333, USA. E-mail address:
11 david.bell@usda.gov

12 ⁴ Jet Propulsion Laboratory, California Institute of Technology, Pasadena, CA 91109, USA. E-mail
13 address: mdplongo@gmail.com; ovidiu.csillik@jpl.nasa.gov

14 ⁵ Climate and Ecosystem Sciences Division, Lawrence Berkeley National Laboratory, Berkeley, CA
15 94720, USA. E-mail address: mlongo@lbl.gov

16 ⁶ Forest Biometrics, Remote Sensing and Artificial Intelligence Laboratory, School of Forest, Fisheries
17 and Geomatics Sciences, University of Florida, Gainesville, FL 32611, USA. E-mail address:
18 c.silva@ufl.edu

19 **Key points**

- 20 ○ Evapotranspiration, surface temperature and forest structure data can inform about the
21 effects of canopy cover changes in the Amazon
- 22 ○ Forest disturbances affect evapotranspiration-temperature relationships differently across
23 wet and dry seasons and disturbance levels
- 24 ○ Forest structure showed moderate relationship with evapotranspiration in heavily
25 disturbed forests and weak correlation at intact forests

26 **Abstract**

27 The Brazilian Amazon has been a focus of land development with large swaths of forests
28 converted to agriculture. Forest degradation by selective logging and fires has accompanied the
29 advance of the frontier and has resulted in significant impacts on Amazonian ecosystems.
30 Changes in forest structure resulting from forest disturbances have large impacts on the surface
31 energy balance, including on land surface temperature (LST) and evapotranspiration (ET). The

32 objective of this study is to assess the effects of forest disturbances on water fluxes and canopy
33 structural properties in a transitional forest site located in Mato Grosso State, Southern Amazon.
34 We used ET and LST products from MODIS and Landsat 8 as well as GEDI-derived forest
35 structure data to address our research questions. We found that disturbances induced seasonal
36 water stress, more pronounced and earlier in croplands and pastures than in forests, and more
37 pronounced in second-growth and recently burned areas than in logged and intact forests.
38 Moreover, we found that ET and LST were negatively related, with a more consistent
39 relationship across disturbance classes in the dry season than the wet season, and that forest and
40 cropland and pasture classes showed contrasting relationships in the dry season. Finally, we
41 found that canopy structural properties exhibited moderate relationships with ET and LST in the
42 most disturbed forests, but negligible correlations in the least disturbed forests. Our findings help
43 to elucidate degraded forests functioning under a changing climate and to improve estimates of
44 water and energy fluxes in the Amazon degraded forests.

45 **Plain Language Summary**

46 Deforestation, selective timber extraction and forest fires are the main causes of forest
47 disturbances in the Amazon region. These disturbances alter how forests function. Forest
48 degraded by logging and fires may exchange less water and absorb less carbon dioxide from the
49 atmosphere during photosynthesis. We used satellite-based observations on the amount of water
50 transpired to the atmosphere by trees (known as evapotranspiration), land surface temperature,
51 and forest structural properties such as canopy cover and height over a region in the Southern
52 Amazon to understand the differences in function between disturbed and intact forests. We found
53 that disturbances induced stronger and earlier water stress in the dry season in croplands and
54 pastures than in forests, and stronger water stress in second growth and recently burned areas
55 than in logged and intact forests. We also found that structural properties show a moderate
56 relationship with evapotranspiration and temperature in the most disturbed forests, but weak
57 relationships in the least disturbed forests. Our findings highlight the importance of intact forests
58 in maintaining water balance in the Amazon region and suggest that disturbed forests may have
59 limited ability to cope with the changing climate.

60 **Keywords**

61 Amazon; forest degradation; forest structure; evapotranspiration; land surface temperature

62

63 **1. Introduction**

64 Changes in tree cover and forest structure have large impacts on energy balance and
65 ecosystem properties, altering components of the biosphere-atmosphere interactions that operate

66 from the leaf (plant physiology) to global (atmospheric circulation) scales. Deforestation and
67 forest degradation can alter rainfall regimes, water availability, and surface-atmosphere flux of
68 water and energy of tropical forests (Davidson et al., 2012; Jucker et al., 2018; Longo et al.,
69 2020; Spracklen et al., 2018). These impacts are particularly pronounced in ecotonal, semi-
70 deciduous tropical forests of the southern Amazon Basin, which have experienced rapid regional
71 warming and deforestation over the last three decades (Vourlitis et al., 2008). However,
72 integrated assessments linking structural and functional changes resulting from forest
73 disturbances are still lacking, and climate and forecast models are incipient in representing the
74 influence of canopy structure on energy and water balances in degraded Amazon forests (Huang
75 et al., 2020; Longo et al., 2020).

76 Chief among the water balance variables, evapotranspiration (ET) is a multi-faceted variable
77 controlled by a combination of vegetation, atmospheric, and radiative drivers. ET measurements
78 need to ensure that the abiotic and biotic controls are adequately captured: net radiation and land
79 surface temperature provide the physical drivers for the state change of water and the subsequent
80 impact on latent and sensible heat partitioning; humidity and air temperature regulate the transfer
81 of water from the land into the air, and phenology and vegetation cover information are
82 necessary for seasonal dynamics and relative magnitudes of ET fluxes (Fisher et al., 2008). One
83 critical measurement to the estimation of remotely-sensed ET is the land surface temperature
84 (LST), as it can capture fine spatial and temporal dynamics associated with heterogeneous land
85 surface processes controlling ET (Fisher et al., 2017).

86 Variability in the strength of ET drivers may be linked to different degrees of the canopy-
87 atmosphere coupling (Jarvis & McNaughton, 1986). The control of ET can be viewed as
88 complex supply-demand interactions, where net radiation and soil moisture represent the supply
89 and the atmospheric vapor pressure deficit (VPD) represents the demand. This supply-demand
90 interaction accelerates the biophysical feedbacks in ET. The degree of biophysical control is a
91 function of the ratio of canopy conductance (an aggregated measure of canopy control on
92 transpiration) to aerodynamic conductance. When the canopy and aerodynamic conductance
93 ratio is very small (i.e., water-stress conditions), stomata principally control the water loss and a
94 change in canopy conductance results in a nearly proportional change in transpiration. Such
95 conditions trigger a strong biophysical control on transpiration. In this case, vegetation is
96 believed to be fully coupled to the atmosphere. In contrast, for a high canopy and aerodynamic
97 conductance ratio (i.e., high water availability), changes in canopy conductance will have little
98 effect on the transpiration rate, and transpiration is predominantly controlled by net radiation
99 (Mallick et al., 2016).

100 In the Amazon basin, ET exerts a large influence on regional and global climate patterns, and
101 provides a significant source of rainfall water in South America (Maeda et al., 2017; Spracklen
102 et al., 2012; van der Ent et al., 2010), by returning to the atmosphere between 50 and 75% of the
103 regional precipitation (Lathuillière et al., 2012; Malhi et al., 2002). The major environmental
104 controls driving spatial and temporal variability of ET in the Amazon are solar radiation
105 (accounting for more than 80% of ET variability), atmospheric VPD, vegetation cover, and
106 precipitation (Fisher et al., 2009), but complex interactions resulting from local climatic and
107 biotic conditions generate highly heterogeneous patterns across the region (Fisher et al., 2009;
108 Hasler & Avissar, 2007; Maeda et al., 2017). Synergies between climate and forest structure and
109 functioning control much of the spatial variability in water and energy balances in the Amazon
110 (Coe et al., 2016). While forest ET increases during the dry season in equatorial Amazonian
111 forests, seasonally dry forests at the southern fringe of the biome present the opposite trend (da
112 Rocha et al., 2009; Hasler & Avissar, 2007; Restrepo-Coupe et al., 2013).

113 Land cover changes alter vegetation cover and structure and land surface properties such as
114 albedo, emissivity, and surface roughness (Bonan, 2008; Bright et al., 2015). Ultimately, the
115 conversion of natural areas to urban or agricultural development affects gas and energy exchange
116 processes between the land surface and the atmosphere, by changing how incoming precipitation
117 and radiation are partitioned among sensible and latent heat fluxes and run-off (Coe et al., 2016).
118 Decreased forest cover increases surface albedo and reduces net radiation and ET (Costa &
119 Foley, 1997). Based on eddy covariance data collected in the Western Amazon, von Randow et
120 al. (2004) found evapotranspiration rates 20-41% lower in pastures compared to forests. Silvério
121 et al. (2015) showed, for a large river basin in the southern Amazon, that abrupt transitions in
122 land uses such as forest/crops and forest/pastures decreased ET by 32% and 24%, respectively.
123 These authors also found that LST was 6.4°C higher over croplands and 4.3°C higher over
124 pasturelands, compared to the forests they replaced. Using an ecosystem demography model
125 calibrated with tropical forest parameters, Longo et al. (2020) estimated that severely degraded
126 forests experience water-stress with ET declines up to 34% and increases in daily mean ground
127 temperatures (up to 6.5° C) relative to intact forests. Seasonality of water and energy fluxes also
128 amplifies differences among disturbed and intact vegetation, due to their differential capability to
129 access subsurface water during seasonal drought (von Randow et al., 2004; Zemp et al., 2017).

130 Disturbed forests in the Amazon are expected to transpire substantially less compared to old-
131 growth forests, because of the potential reductions in LAI and rooting depth (Silvério et al.,
132 2015), but recent research has shown contrasting results. Some degraded forests have shown ET
133 levels similar to intact forests' or even increased ET after a few years after fires or start of the
134 secondary growth, with no corresponding recovery in structural attributes such as biomass or leaf

135 area index (LAI) (Brando et al., 2019; Von Randow et al., 2020). Canopy structural properties
136 are intrinsically affected by disturbance type, intensity, and time since events. Given that
137 changes in tree cover and structure have large impacts on energy balance and ecosystem
138 properties, there is an urgent need to quantify these properties not only for mature forests but
139 also for forests with lower, less complex cover and structure.

140 Active and optical remote sensing approaches have been widely used to directly observe or
141 estimate LST, ET and forest structural properties. The ET product from the Moderate Resolution
142 Imaging Spectroradiometer (MODIS) is estimated using the Penman-Monteith equation
143 (Monteith, 1965) and utilizes other MODIS products and meteorological inputs. While MODIS
144 has long run and well-established ET products, its coarse resolution may not be adequate to
145 capture the ET variability associated with small scale disturbances. Therefore, we also used ET
146 derived from Landsat 8 data, retrieved as a residual of the surface energy balance (SEBAL
147 algorithm; Bastiaanssen et al., 1998), and using LST observations as the most important input.
148 Landsat is distinguished by being both the first medium resolution Earth observation satellite as
149 well as the longest running continuous program, with the recent Landsat launches showing
150 improved geometric and radiometric properties (Wulder et al., 2019). Laser scanning, an active
151 form of remote sensing commonly known as lidar, is suitable to characterize three-dimensional
152 forest structural properties (Lefsky et al., 2002). The Global Ecosystem Dynamics Investigation
153 (GEDI) spaceborne lidar instrument has been providing unprecedented three-dimensional
154 information of tropical and temperate forests worldwide (Dubayah et al., 2022; Dubayah et al.,
155 2020; Duncanson et al., 2022) and has made it possible to investigate forest structure over large
156 areas in the Amazon.

157 The objective of this study is to assess the effects of forest disturbances (both
158 deforestation/total canopy cover removal and degradation/partial canopy cover removal) on the
159 seasonal ET fluxes and canopy structural properties in a transitional forest site located in Mato
160 Grosso State, Southern Amazon. We use ET and LST data from MODIS and Landsat 8 OLI and
161 TIRS sensors, taking advantage of their well-established record in the investigation of water
162 fluxes (Anderson et al., 2012; Mu et al., 2011), as well as the novel GEDI forest structure data
163 (Dubayah et al., 2022) to address the following questions: a) What is the effect of forest
164 disturbances on the seasonal water stress of the canopy? b) How are variations in seasonal water
165 stress manifested in LST-ET relationships across the study site, and do these relationships vary
166 with season and disturbance severity levels? c) What is the contribution of canopy structural
167 properties to ET and LST? Table 1 summarizes our research questions and related hypotheses,
168 and the datasets used to address each of them.

169

Research questions	Hypotheses tested	Datasets used
Q1. What is the effect of forest disturbances on the seasonal water stress of the canopy?	H1. Areas with decreased vegetative cover exhibit reduced ET earlier in the dry season, with equivalent water stress	MODIS MYD16A2 product (Total Evapotranspiration and Total Potential Evapotranspiration layers), 1 year of 8-day composites at 500-m resolution.
Q2a. How are variations in seasonal water stress manifested in LST and ET relationships in the study site?	H2.a. LST is higher in areas with low ET and canopy cover	Landsat 8 LST, Landsat 8 ET (derived from the METRIC model), wet and dry season single dates at 30-m resolution
Q2b. Do these relationships vary with seasons and disturbance level?	H2.b. The negative ET-LST relationship will be stronger in more severely disturbed forests and during periods of greater water stress	
Q3.a. What is the contribution of canopy structural properties to ET and LST?	H3.a. ET and LST covaries with structural properties in Amazon disturbed forests	Landsat 8 LST, Landsat 8 ET (derived from the METRIC model), dry season single date at 30-m resolution Structural properties (canopy cover, plant area index, top-of-canopy height, and foliage height diversity) from GEDI at 25-m footprint

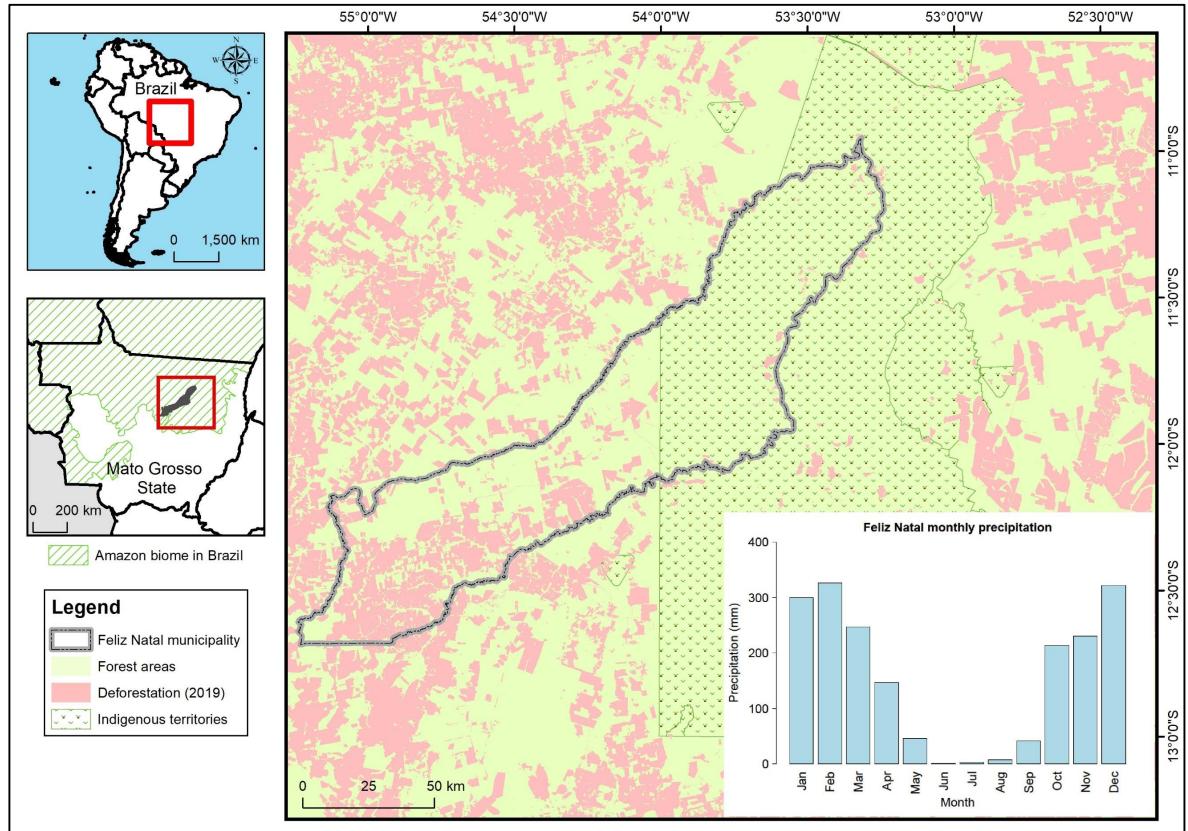
171

172 2. Material and methods

173 2.1. Study area

174 The study area covers approximately 100,000 km² at the southern and drier flank of closed-
 175 canopy Amazon forests in the Brazilian state of Mato Grosso (Figure 1), including the
 176 municipality of Feliz Natal. The area is covered by evergreen broadleaf forests (IBGE, 2021). A
 177 five-month dry season (May to September) accounts for only 6% of mean annual precipitation
 178 (inset in Figure 1).

179 This site is located in the ‘Arc of deforestation’, a region that surrounds the southern edge of
 180 the Amazon biome, where conventional practices include land clearing for cattle ranching,
 181 small-scale subsistence farming, logging, and, increasingly, soybean production for global
 182 markets. Decades of agricultural expansion (which includes fire as a land clearing technique) and
 183 selective logging have left a mosaic of fragmented and degraded forests in the area (Matricardi et
 184 al., 2010; Morton et al., 2013; Souza et al., 2005), with the majority of intact forests remaining
 185 inside the indigenous reserves (Figure 1).



187

188 Figure 1. Location, forest cover and monthly precipitation (inset) of the study area. Source of precipitation data:
 189 climate-data.org. Source of deforestation data: INPE (2020).

190 2.2. Disturbance history assessment

191 We mapped the land cover/land use of the Feliz Natal region from 2000 to 2018, including
 192 both disturbances that lead to degradation of standing forests (selective logging and fires) and
 193 classes of land use that follow stand-replacement disturbances (croplands, pastures and
 194 secondary forests). To map forest degradation, we masked out accumulated deforestation until
 195 2019 (INPE, 2020) and areas of alluvial vegetation. Subsequently, we mapped logged and
 196 burned areas on the forest remnants based on visual interpretation of yearly fitted Normalized
 197 Burn Ratio (NBR) images derived from Landsat 5, 7, and 8 observations. To differentiate forests
 198 experiencing variable degrees of disturbance, we classified degraded forests into six classes: 0-3
 199 years (L1), 4-7 years (L2), and 8-14 (L3) years after logging, and 0-3 years (B1), 4-7 years (B2),
 200 and 8-14 (B3) years after burning, while forested areas with no signs of logging or fires in the
 201 time-series were classified as intact forests (IN). Polygons that experienced multiple degradation
 202 events in the time-series were classified according to the latest event. Details of the methodology
 203 for mapping intact and degraded forests can be found in Rangel Pinagé et al. (2022).

204 Subsequently, we included classes of land cover following deforestation in the disturbance
 205 history. Crop (CR) and pasture (PA) polygons for 2019 were obtained from the MapBiomas
 206 Collection 5 data of Brazil's annual land cover and use maps, based on Landsat images

207 (MapBiomias Project, 2019). Also from MapBiomias data, we extracted a land cover class
208 representing the transition of pasture and crops to forest cover from 2015 to 2019 to represent
209 young secondary forests (SFN). Next, we extracted data for the old secondary forest class (SFO)
210 from the TerraClass dataset, which classifies land uses following deforestation in the Amazon,
211 based on Landsat and MODIS data. We chose to use TerraClass until 2014 instead of the
212 regeneration data from MapBiomias because the former is more consistent with the INPE
213 methodology for deforestation mapping (Almeida et al., 2016).

214 The consolidated layer of disturbance history was generated by merging the forest
215 degradation, old secondary forest (from TerraClass), and crop/pasture and young secondary
216 forest (from MapBiomias) individual layers (Figure 2). We eliminated isolated polygons with
217 areas smaller than 50 hectares to be consistent with MODIS resolution.

218 **2.3. Remote sensing data**

219 The remote sensing data employed in this study includes ET modelled from MODIS
220 observations, ET (modeled) and LST from Landsat 8 observations, and forest structural
221 properties from GEDI observations.

222 *2.3.1. MODIS data*

223 Due to its high temporal resolution and compositing scheme, MODIS data allow for the
224 generation of consistent seasonal patterns. To address Q1, we used the MYD16A2 Version 6
225 Evapotranspiration/Latent Heat Flux product, an 8-day composite dataset produced at 500-m
226 resolution (Running et al., 2017). The layers ET_500m (for total evapotranspiration) and
227 PET_500m (for total potential evapotranspiration) were selected, along with the quality control
228 flag layer to filter out low-quality data. The improved algorithm of product MYD16A2 is based
229 on the logic of the Penman-Monteith equation, which includes inputs of daily meteorological
230 reanalysis data along with MODIS data products such as vegetation property dynamics, albedo,
231 and land cover. The pixel values for the ET and PET layers represent the sum of all eight days
232 within the composite period.

233 To test the hypothesis that areas with low forest cover experience water stress earlier in the
234 dry season (H1), we applied the concept of Evaporative Stress Index (ESI, Fisher, 2013),
235 computed from the ratio between actual and potential evapotranspiration. Any ET less than the
236 PET is an indicator that water supply is limited; plants may close stomata to conserve water, and
237 productivity may therefore be less than optimal. Hence, the actual-to-potential ET ratio
238 (ET/PET) is a key indicator of plant water stress (low values of ESI are associated with increased
239 water stress, and high ESI values are associated with lack of water stress). Moreover, anomalies
240 to ET/PET can provide valuable information about water stress without requiring precipitation or

241 soil moisture information (Anderson et al., 2012). We divided the ET by the PET layer, extracted
242 the pixels over the polygons of each disturbance class, and finally, extracted their mean values
243 for each 8-day composite to build the 2019 annual profile of ESI.

244 2.3.2. Landsat 8 OLI and TIRS data

245 While MODIS ET estimates are valuable for understanding spatially integrated regional ET
246 patterns and seasonality, they are not able to capture fine-scale spatial dynamics associated with
247 heterogeneous land surface processes controlling ET. Hence, to address Q2 and Q3, which are
248 related to relationships of ET with LST and forest structure, we used Landsat data at 30-m
249 resolution over a ~ 300,000-hectare subset (approximately 3.5% of the total area, yellow outline
250 polygon in Figure 2) within the same image scene. Using one single scene minimizes
251 inconsistency of ET values across disturbance classes. For Q2, we compared ET and LST
252 relationships across disturbance classes at single dates at the wet (January 31st, 2019) and dry
253 (September 28th, 2019) seasons. For Q3, we used the ET and LST data from September only
254 along with structural variables from GEDI (described in the next section). We used only one dry
255 season date to compare ET and LST relationships with forest structure data because the latter is
256 not expected to change seasonally or daily, unlike process variables such as evapotranspiration
257 or gross primary productivity.

258 Land surface temperature and evapotranspiration data were derived from Landsat 8
259 observations. The images were obtained through the Earth Engine Evapotranspiration Flux
260 (EEFlux version 0.20.3, described at Allen et al. (2015)). EEFLUX is based on the Mapping
261 Evapotranspiration at High Resolution Internalized Calibration (METRIC) (Allen et al., 2007).
262 Within EEFLUX workflow, LST data is generated using a fixed atmospheric calibration, where
263 the near-surface temperature gradients are an indexed function of radiometric surface
264 temperature, thereby eliminating the need for absolutely accurate surface temperature and the
265 need for air-temperature measurements. Actual evapotranspiration is derived from the Landsat
266 images representing the 24-hour actual ET, via the standard automated calibration within
267 EEFlux. In this framework, actual ET is calculated as a residual of the surface energy balance,
268 according to the following equation:

$$LE = R_n - H - G$$

269 where: LE is the latent heat flux (energy spent in the evapotranspiration process (W m^{-2}); R_n is
270 net radiation (W m^{-2}); G is the heat flux in the soil (W m^{-2}), and H is the sensible heat flux (W
271 m^{-2}). The EEFlux calibration uses the Landsat thermal band and shortwave bands to estimate the
272 surface energy balance and to estimate the amount of vegetation, albedo and surface roughness.
273 Version 0.20.3 of EEFlux employs automated image calibration by assigning values for EToF

274 (which represents ET as a fraction of the reference evapotranspiration) for the 'hot' and 'cold'
275 pixels of the surface temperature spectrum of the scene. LE is estimated at the exact moment of
276 the passage of the satellite for each pixel and instantaneous ET is then calculated by dividing the
277 LE by the latent heat of vaporization, according to the following equation:

$$ET_{inst} = 3600 LE / \lambda \rho_w$$

278 where: ET_{inst} is the instant evapotranspiration (mm h^{-1}); 3600 converts seconds to hours; λ is the
279 latent heat of vaporization (J kg^{-1}), and ρ_w is the density of water ($\sim 1000 \text{ kg}^{-3}$). Numata et al.
280 (2017) assessed the accuracy of METRIC ET estimates for the Amazon region and found good
281 agreement between METRIC and flux tower-derived ET ($R^2 > 0.7$).

282 To assess the ability of Landsat data to capture the seasonal water stress detected with
283 MODIS, we chose two Landsat images of a subset of the study area (yellow polygon in Figure 2)
284 from the wet and late dry seasons with the least cloud coverage and extracted the equivalent of
285 an ESI (ratio of actual and reference ET).

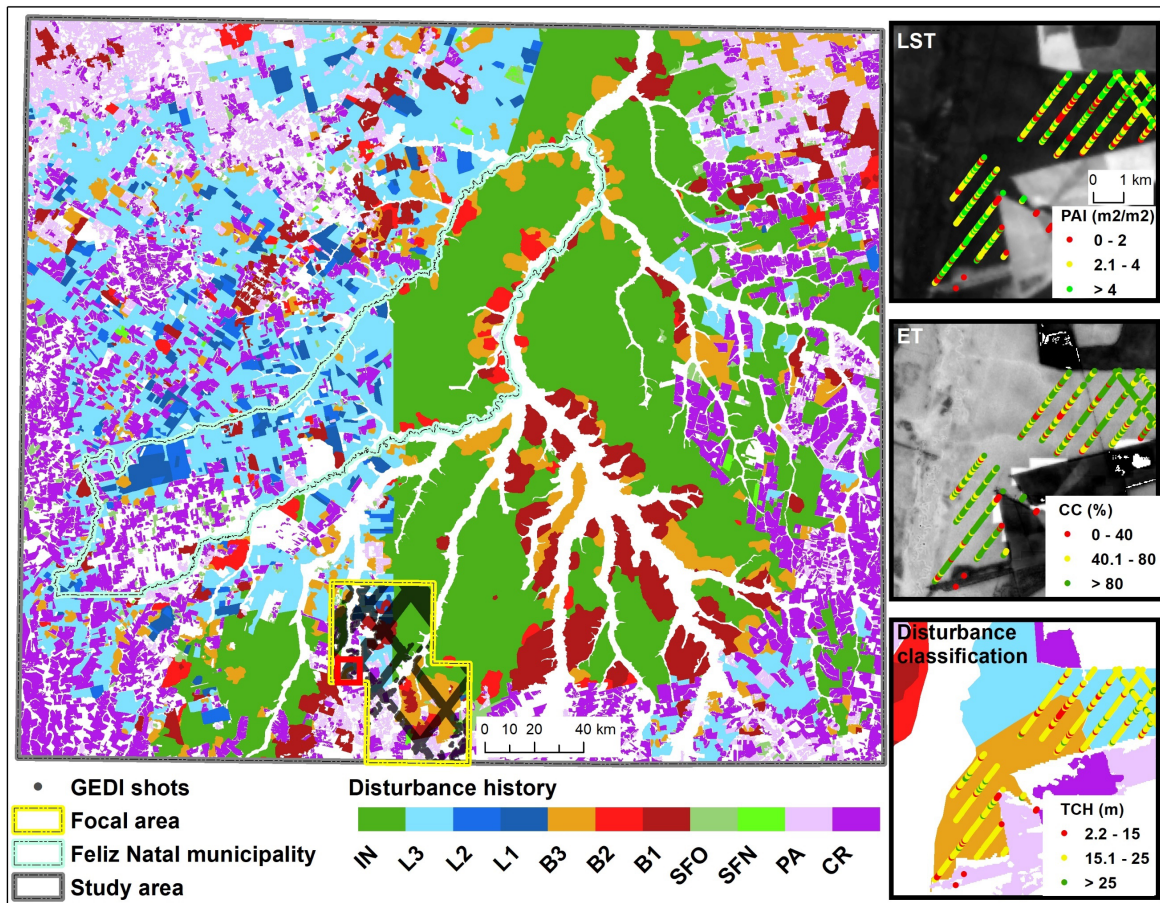
286 2.3.3. GEDI data

287 GEDI produces high resolution 3D observations of Earth's forests and topography (Dubayah
288 et al., 2020). GEDI's precise measurements of forest canopy height, canopy vertical structure,
289 and surface elevation at a 25-meter footprint can characterize important carbon and water
290 cycling processes, biodiversity, and habitat (Dubayah et al., 2020).

291 To address Q3, we extracted four structural properties from GEDI Level 2A and 2B data: top
292 of canopy height (TCH, m), plant area index (PAI, m^2/m^2), canopy cover (CC, %) and foliage
293 height diversity (FHD, unitless). TCH was derived from level 2A data (GEDI L2A Canopy
294 Elevation and Height Metrics). The RH98 (the 98th percentile return height) was used as a proxy
295 for TCH. PAI, CC and FHD were derived from Level 2B (GEDI L2B Footprint Canopy Cover
296 and Vertical Profile Metrics) (Tang & Armston, 2019).

297 We processed the version 2 of GEDI Level 2A and Level 2B data for the study area, for the
298 period between May 5 and November 11, 2019. To filter low-quality data, we only kept laser
299 shots with the recommended quality flags (i.e., sensitivity ≥ 0.95 , quality flag = 0, and degrade \neq
300 0; Hofton et al., 2019). We implemented an additional filter to remove data in the adjacency of
301 low-quality data, by keeping the shots along a single beam that were part of a continuous strike
302 of at least 30 good quality filtered shots. Finally, we excluded additional shots within fire scars
303 detected in 2019 according to the DETER-B datasets (Diniz et al., 2015) and without associated
304 values of ET or LST (i.e., due to cloud on Landsat observations). After the application of all
305 filters, a total of 12,551 shots from the subset of the study area were retained (Figure 2). GEDI

306 data processing was performed in a Geographic Information System (GIS) platform and the R
 307 statistical software (R Core Team, 2021), with the aid of the rGEDI package (Silva et al., 2020).



308
 309 Figure 2. Disturbance classification at Feliz Natal region and post-filtered GEDI shots over the focal area (yellow
 310 outline polygon). Insets are zooms from the red outline polygon in the main map and show GEDI structural
 311 properties (PAI, CC and TCH). Inset background images are LST and ET from Sep-2019. Higher values of LST and
 312 ET are brighter. Unclassified areas (over alluvial vegetation or savannas, or due to mismatch among input datasets)
 313 are shown in white in the disturbance classification.

314 2.4. Statistical analysis

315 To compare ET and LST among the disturbance classes and across seasons, we applied the
 316 Tukey’s Honestly Significant Difference test (henceforth Tukey’s test) (Tukey, 1977) to identify
 317 statistically distinct groups.

318 To assess ET-LST relationships, we developed linear regression models with ET as the
 319 dependent variable. The models were fit at the pixel level for dry and wet seasons for the
 320 disturbance classes separately. We did not fit models for the data encompassing all classes
 321 because the ET-LST relationship in that case was clearly nonlinear. In addition, we tested the
 322 differences in slope coefficients between wet and dry seasons for each group to evaluate how
 323 seasonal moisture stress influences the relationship between ET and LST. Only 1/500 pixels
 324 were included in the regression models, and observations falling below the 2.5th and above the

325 97.5th percentiles were excluded, to minimize outliers that are likely to occur in the edges of
326 polygons from the different classes.

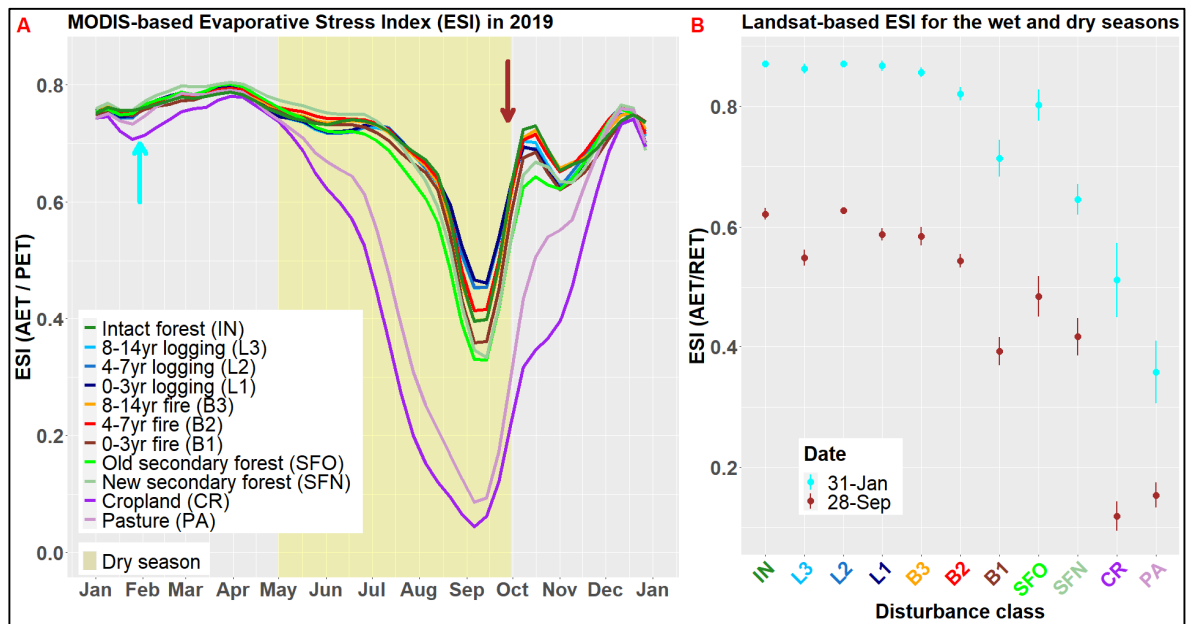
327 To compare GEDI-derived structural properties among the disturbance classes, we also used
328 violin plots and the Tukey's test to compare all possible pairs of means. Next, we fitted linear
329 regression models at the GEDI footprint level with ET and LST as dependent variables and each
330 structural attribute as the independent variable, to assess the relationship between ET or LST
331 with structural variables. We made no assumptions on the normality or transformation of the
332 data due the large sample size (> 1000 observations). All statistical tests, analysis and plotting
333 were performed in the R statistical environment (R Core Team, 2021).

334 3. Results

335 3.1. Seasonal water stress

336 The 2019 annual profile of the ESI showed that forest and non-forest classes in Feliz Natal
337 region experience year-round ESI < 1 (Figure 3). The disturbance classes showed varied
338 evaporative stress in the dry season (May through September) and could be distinguished into
339 two groups with well-marked water stress signals: croplands and pastures and forests (Figure 3).

340 Croplands and pastures exhibited the sharpest ESI decline at the onset of the dry season,
341 with ESI almost reaching zero (meaning maximum evaporative stress or no vegetation cover) at
342 the end of the dry season (Figure 3A). Pastures showed a similar annual pattern to that of
343 croplands but with a less pronounced ESI decrease.



344
345 Figure 3. Annual profile of the MODIS Evaporative Stress Index for the disturbance classes for Feliz Natal region
346 (A). The cyan and brown arrows in A indicate the dates that the Landsat-based ESI for a subset of the study area
347 was extracted (B). A sample of 100 Landsat pixels was included for each class. The error bars in B represent 95%

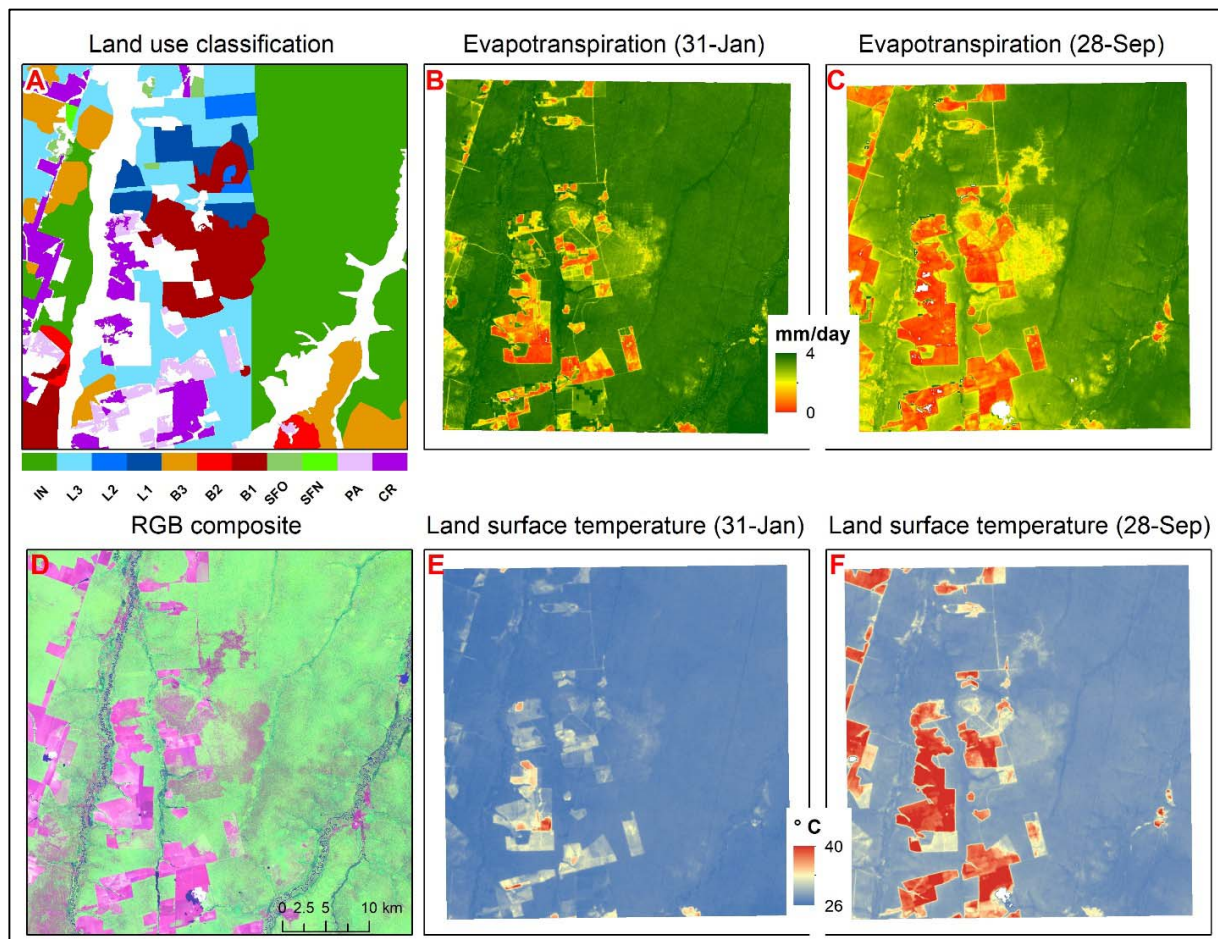
348 confidence interval of the mean. Labels in the x-axis in B represent the disturbance classes and are in the same order
349 and color of the legend in (A).

350 ESI from the different forest classes declined sharply later in the dry season, and with a much
351 weaker descent than crops and pastures. Among the forest classes, logged forests showed higher
352 ESI than intact forests at the time of the most severe water stress signal in early September (0.45-
353 0.46 and 0.39, respectively). Recently burned forests showed lower ESI than intact forests
354 (0.36), whereas the older burned classes showed similar or higher ESI compared to intact forests
355 (0.39-0.41). Meanwhile secondary forests showed slightly lower ESI values compared to the
356 other forest classes (~ 0.33). Interestingly, pastures and croplands showed similar MODIS-based
357 ESI levels as that of forests during most of the wet season (Figure 3A).

358 Water stress in the late dry season (in September) is also detected by Landsat data (Figure
359 3B), but with improved water stress discrimination among classes (e.g., larger differences within
360 burned and secondary forests). However, Landsat data showed larger differences between the
361 least and most disturbed classes in both seasons with substantially lower ESI values for
362 croplands and pastures, while MODIS ESI showed little divergence in the wet season (Figure
363 3A). Landsat's finer spatial resolution is likely producing this better discrimination, but it could
364 be due to different sensor's characteristics and ET retrieval algorithms.

365 **3.2. ET-LST relationships**

366 By using Landsat observations of land surface temperature (LST) and evapotranspiration
367 (ET), we found that some areas of croplands and pasturelands show moderate ET in January (wet
368 season), comparable to degraded forests, and that ET differences within degraded and intact
369 forests are amplified in September (dry season). LST in the other hand shows higher values in
370 crop and pasturelands in both analyzed periods, but with notably higher differences compared to
371 forests in the dry season (Figure 4).

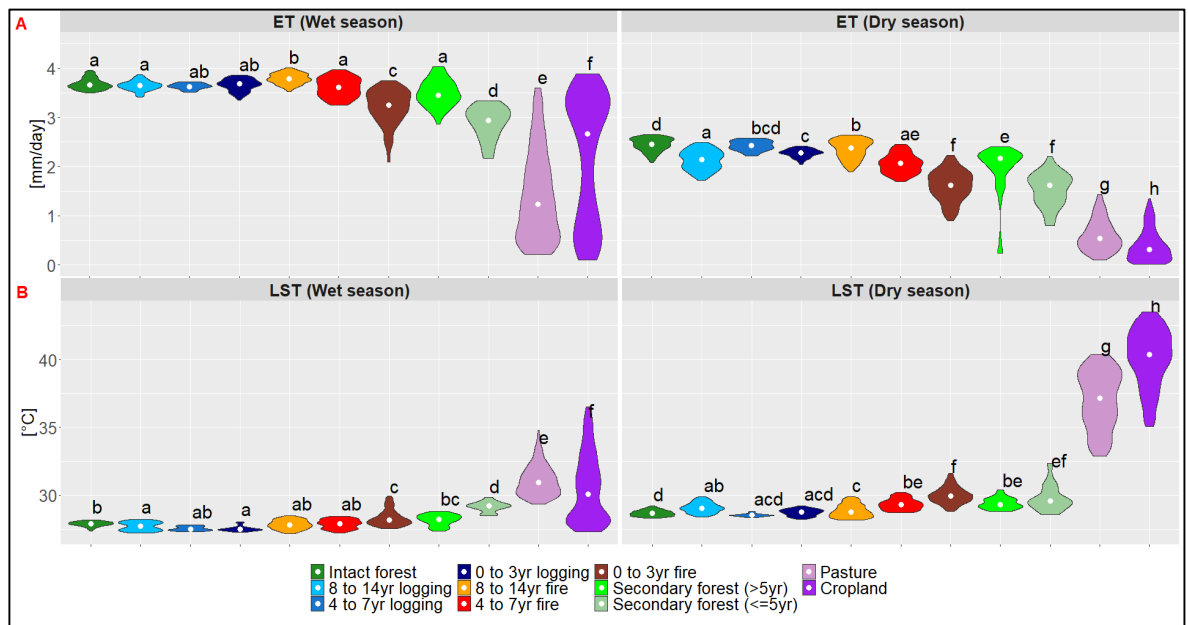


372

373 Figure 4. Disturbance classification (A), evapotranspiration in wet and dry seasons (B-C), a false-color RGB
 374 composite image (D), and land surface temperature in wet and dry seasons (E-F) over a subset of the study area. RGB
 375 composite image info: Landsat 8, path/row 225/069, date 28-Sep-2019, R6G4B5. ET and LST data are from
 376 EEFLUX.

377 The seasonal variation in ET and LST was largely consistent with the continuum of
 378 disturbance intensity (Figure 5, sorted from intact forests to crops). ET and LST were inversely
 379 correlated, showing opposite trends in both wet and dry season dates. In January, most forest
 380 classes showed similarly high ET ranges (median: 3.4-3.8), except for the most recent burned
 381 and secondary forests (median: 3.2 and 2.9, respectively) (Figure 5A). Croplands and pastures
 382 showed greater variability than forests, but croplands exhibited a high proportion of pixels with
 383 high ET as well (median: 2.6 and 13, respectively). Toward the end of the dry season (e.g.,
 384 September), following maximum evaporative stress (Figure 3), ET and LST in pasture and
 385 croplands patterns were distinct from all forest classes. Forests also showed increased
 386 differentiation in the dry period compared to the wet season. LST showed a similar pattern of
 387 differentiation among the classes, but an opposite trend of values (higher in those classes with
 388 lower ET estimates, Figure 5B).

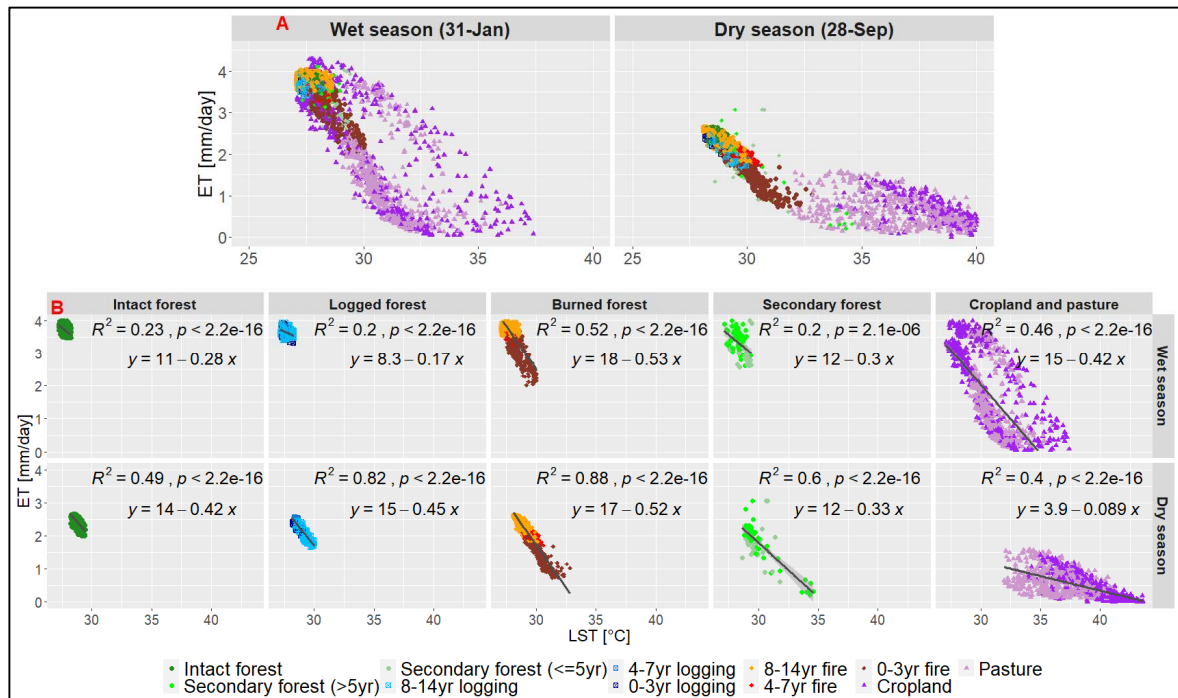
389



390

391 Figure 5. Distribution of ET (A) and LST (B) in the wet and dry seasons across the disturbance classes. Only 1/500
 392 pixels were included, and observations falling below the 2.5th and above the 97.5th percentiles were excluded. Violin
 393 plots show the kernel probability density of the data at different values. All violins have the same width, and the
 394 median of each group is indicated by the white dots. Groups labelled with the same letter are not significantly
 395 different at a confidence level of 95% (Tukey's HSD test). The wet season image date is January 31st, 2019, and the
 396 dry season image date is September 28th, 2019.

397 We found a strong negative relationship between ET and LST across disturbance classes,
 398 with a global correlation coefficient of -0.81 (Figure 6). Two clusters of points were observed in
 399 the dry season data: forest classes at one end (with intact forests at the edge of this cluster), and
 400 crops and pastures at the other end. In the wet season data, there is no such clear differentiation:
 401 ET from cropland and pastures is more variable, with the highest values being like those
 402 observed in forests. Moreover, the secondary forest classes mostly had their points spread in the
 403 transition between the two clusters in the dry season.



404

405 Figure 6. Relationship between ET and LST in wet and dry seasons for all classes (A), and for the broad disturbance
 406 classes separately (B). 1/500 pixels were randomly included, and observations falling below the 2.5th and above the
 407 97.5th percentiles were excluded. Black lines represent the best fit line.

408 To assess ET and LST relationships over different land cover types, we merged the
 409 disturbance classes into five broad classes, namely intact, logged, burned and secondary forests,
 410 and crops and pastures (Figure 6B). All the regression models were significant, but the
 411 regression coefficients varied widely. Dry season conditions strengthened ET-LST relationship
 412 (i.e., increased the coefficient of determination, R^2) in intact, logged, burned and secondary
 413 forests. Nevertheless, in terms of sensitivity of the relationship (i.e., the slope coefficient),
 414 burned and secondary forest classes showed very small or not significant differences in slope
 415 across seasons (Table 2). Croplands and pastures were the only class that showed a lower
 416 coefficient of determination, and a much lower slope in the dry season.

417 All classes showed significantly different slopes between wet and dry seasons (p -value <
 418 0.05), except secondary forests (p -value = 0.72), whereas the largest difference was observed at
 419 the cropland and pasture class (Table 2). A significant finding is that intact and logged forests
 420 showed a positive difference in trend (significantly higher slope in the dry season), whereas
 421 burned and secondary forests showed a negative trend (implying smaller slopes in the dry
 422 season, but with non-significant or marginally significant differences).

423

424

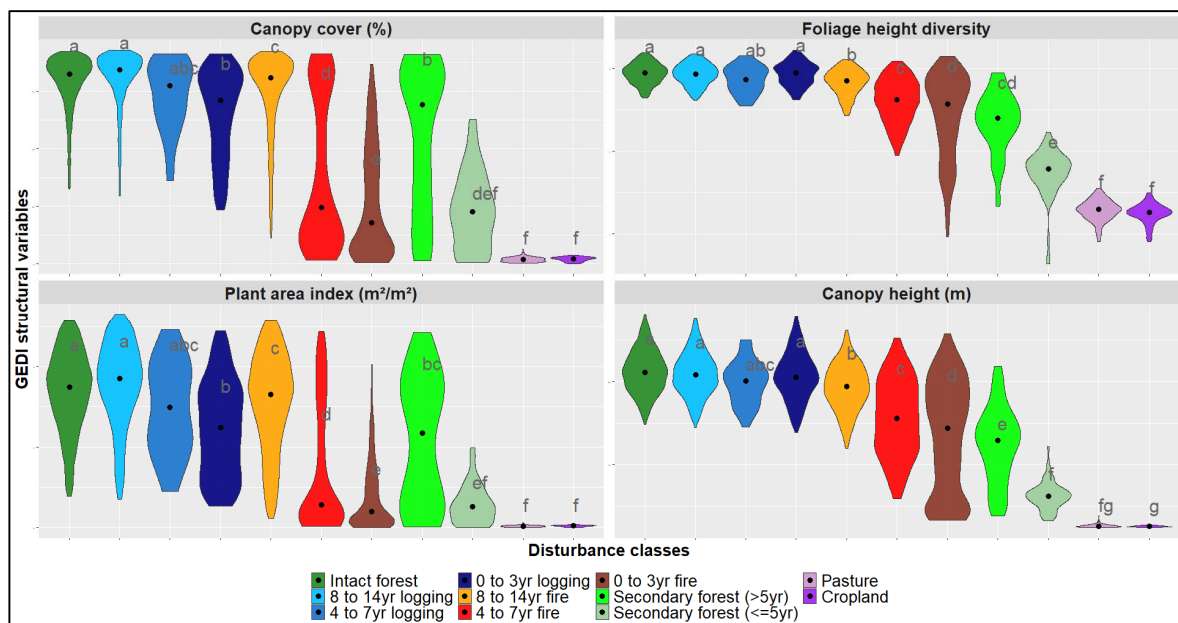
425 Table 2. Estimates of slope differences between wet and dry season in ET and LST relationship for the broad
 426 disturbance classes. P-values of pairwise comparisons > 0.05 (highlighted in gray) indicate non-statistically
 427 significant differences in slope at 95% confidence level.

Pair	Difference in trend	SE	df	t.ratio	p.value
Intact forest	0.149	0.0182	2577	8.205	<.0001
Logged forest	0.282	0.0149	1248	18.948	<.0001
Burned forest	-0.041	0.0133	2917	-3.087	0.002
Secondary forest	-0.025	0.0710	202	-0.358	0.720
Cropland and pasture	-0.350	0.0138	1992	-25.363	<.0001

428

429 3.3. Structure-function relationships

430 Forest structural properties derived from GEDI observations over all disturbance classes
 431 were significantly affected by disturbances. Classes following deforestation (secondary forests,
 432 croplands, and pastures) showed the most pronounced responses in the structural properties
 433 assessed (Figure 7). For both canopy cover (CC) and plant area index (PAI), intact forests
 434 showed the highest values, crops and pastures showed the lowest values and the least dispersed
 435 range, whereas young secondary forests showed intermediate values and the broadest range.
 436 Burned and logged forests clearly responded to time since disturbance and disturbance type, as
 437 indicated by increasing CC and PAI with time since disturbance. Young secondary forests (≤ 5
 438 years) showed CC and PAI similar to the most recent burns. FHD, a measure of structural
 439 complexity, showed very little variability among intact and logged forests, whereas burned and
 440 secondary forests and crops/pastures differed significantly from those classes. Except for the
 441 FHD metric, young secondary forests had all GEDI structural metrics not significantly different
 442 from crops and pastures.



443

444 Figure 7. Structural properties derived from GEDI data for the disturbance classes. Groups labelled with the same
 445 letter are not significantly different at a confidence level of 95% (Tukey's HSD test). Observations falling below the
 446 2.5th and above the 97.5th percentiles were excluded.

447 To assess the relationships between structural properties and ET and LST, we grouped the
 448 disturbance classes into four broad categories: intact, logged, burned and secondary forests.
 449 Croplands and pastures were excluded from this analysis because the structure in these classes
 450 might be ephemeral (i.e., crops are harvested), making the examination of relationships of
 451 structure to ET and LST less meaningful.

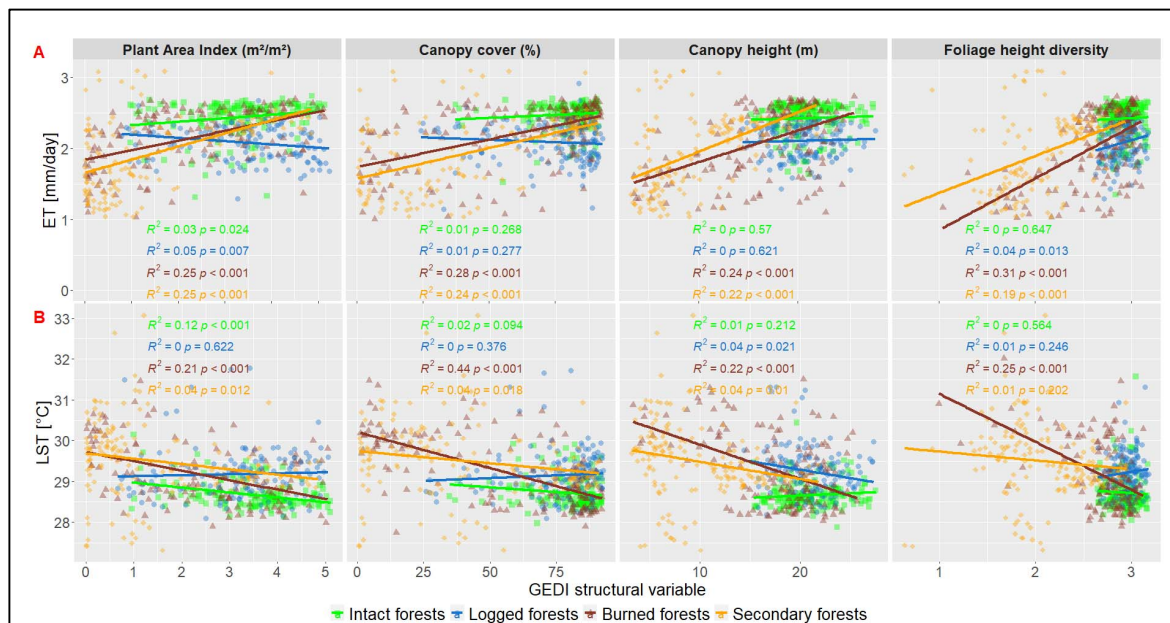
452 Structural properties showed moderate to high correlations with ET (positively correlated,
 453 coefficients from 0.50 to 0.59) and LST (negatively correlated, coefficients from -0.50 to -0.76)
 454 (Table 3). The strongest relationships between structure and ET and LST were observed in the
 455 most intensively disturbed classes (burned and secondary forests), whereas intact and logged
 456 forests showed no significant slopes in the relationships. For instance, CC explained 28 and 44%
 457 of ET and LST in burned forests, and PAI explained 25% of ET in burned and secondary forests.
 458 The greater regression slope for burned and secondary forests compared to intact and logged
 459 forests was consistent across all GEDI-derived structural properties (Figure 8).

460

461 Table 3. Correlation matrix of structural properties with ET and LST. All correlations are significant at 99%
 462 confidence. Positive coefficients are shown in blue and negative coefficients are shown in red.

	Canopy height	Canopy cover	PAI	FHD	ET	LST
Canopy height	1.00	0.79	0.71	0.93	0.56	-0.67
Canopy cover		1.00	0.95	0.74	0.59	-0.62
PAI			1.00	0.63	0.50	-0.50
FHD				1.00	0.58	-0.76
ET					1.00	-0.77
LST						1.00

463



464

465 Figure 8. Relationship between GEDI structural properties and evapotranspiration (A) and land surface temperature
 466 (B) for the broad forest classes. Lines represent the best fit from the linear regression models.

467 ET and LST varied substantially among classes at the lower end of forest structure (short or
 468 low PAI forests), but not at the upper end (tall or high PAI forests) (Figure 8). There was a
 469 separation across the classes because intact and logged forests do not have the extremely low
 470 PAI, CC, canopy height and FHD. Interestingly, ET and LST have different ranges between
 471 intact and logged versus secondary and burned forests with similar PAI or canopy cover at the
 472 intermediate values. Moreover, the regression analysis suggests that most variation in ecosystem
 473 function (ET and LST) from these heavily disturbed forests can be explained by structure,
 474 whereas there is much lower variation in the least disturbed forests explained by structure and
 475 disturbance.

476 4. Discussion

477 In this study, we employed a novel combination of MODIS, Landsat and GEDI observations
 478 to compare seasonal water stress and ET-LST relationships over a continuum of disturbance
 479 conditions; and to quantify the contribution of forest structure properties to ET and LST
 480 variability in secondary, degraded and intact forests. The results showed that disturbances
 481 increased seasonal water stress, earlier and more pronounced in croplands and pastures than in
 482 forests, and more pronounced in second-growth and recently burned areas than in logged and
 483 intact forests. Moreover, we found that the negative ET- LST relationships were more consistent
 484 across disturbance classes in the dry season, and that the forest and cropland & pasture classes
 485 showed contrasting relationships in the dry season. Finally, we found that structural properties of
 486 the canopy such as plant area index, canopy cover, canopy height, and foliage height diversity

487 exhibited moderate relationships with ET and LST in the most disturbed forests, but negligible
488 correlations at the least disturbed forests.

489 **4.1. Water stress, ET and LST variability across a disturbance continuum**

490 The ESI seasonal profile analysis indicated that, while forest classes still showed some
491 divergence in water stress especially at the end of the dry season, pastures and croplands in our
492 study region are highly seasonal with a growing season-dependent exclusively on rainfall (Arvor
493 et al., 2014) (Figure 3). This contrasting pattern occurs because the maximum rooting depth of
494 these crops and grasses is far shallower than those of forests (Nepstad et al., 1994; O'Connor et
495 al., 2019). But certainly, the most novel results of our study are those related to the behavior of
496 secondary-growth and burned forests, showing that they experienced moderate and delayed
497 water stress compared to intact and logged forests, related to changes in structural properties of
498 these forests caused by disturbances (assessed with GEDI data) and potentially to species
499 composition shifts (not assessed in this study).

500 ET generally increased and LST generally increased in the disturbance classes along a
501 disturbance intensity continuum (intact forests < logged forests < burned forests < secondary
502 forests < croplands & pastures). Although studies assessing ET and LST relationships in tropical
503 forests are rare, the dry season declines in ET and increases in LST observed in this study
504 (Figure 5 and Figure 6) agree with similar comparisons in the southern Amazon. Hasler and
505 Avissar (2007) found 5-10% decreases in flux tower -measured ET in the dry season at sites in
506 Rondônia and Mato Grosso States, while (von Randow et al., 2004) found 25% less ET in
507 pastures in Rondonia state during the dry season. In general, we found similar trends, but more
508 pronounced ET declines from January to September (33-40% at intact and least disturbed sites,
509 and even greater declines (~50%) for the most heavily degraded forests, with crops and pastures
510 showing the largest differences (60-80%), and greatest variability (Figure 4, Figure 5, Figure 6).
511 These differences in magnitude could be due to the different methods of data acquisition (e.g.,
512 flux tower data versus satellite-based estimates, or single flux tower sites versus patch averages
513 within a large area). Other plausible explanation for these differences is that the aforementioned
514 studies used data from the early 2000's, while we looked at data from 2020. Temperatures and
515 VPD increased in this interval, which could be adding more stress to these forests
516 (Barkhordarian et al., 2019; Da Silva et al., 2019).

517 Despite slightly reduced PAI (Figure 7), the least disturbed forests such as logged and oldest
518 burns showed ET and LST comparable to intact forests during both seasons (Figure 5),
519 suggesting that albedo and net radiation on these forests recovered or never shifted from that of
520 intact forests. Classes with intermediate levels of disturbance (4-7 yr fires and old secondary

521 forests) showed stronger ET depletion during the dry season, and the most heavily degraded
522 classes (0-3yr fire and young secondary forests) exhibited significantly lower LST and ET
523 compared to intact forests on both seasons. These results agree with Miller et al. (2011), that
524 found modest and ephemeral effects on the water and heat fluxes in a logged forest site in
525 Central Amazon, with changes due to logging smaller than the interseasonal and interannual
526 variability; these authors also found albedo not being significantly affected by logging activities.
527 Similar to our results for burned forests, Brando et al. (2019) found that ET had fully recovered
528 seven years after experimental fires in the same region. Comparing ET between intact and 20-
529 years old secondary forests in Central Amazon, Von Randow et al. (2020) found that secondary
530 forests showed ET approximately 20% higher than primary forests over wet and dry seasons.
531 Given the shorter and less severe dry season in Central Amazon compared to Feliz Natal region,
532 it is reasonable to expect lower ET in the dry season in Feliz Natal. Moreover, our samples
533 include a much larger spatial variability of secondary forest conditions.

534 The strongest (negative) ET-LST relationships were observed at the disturbance classes with
535 larger ranges of ET and LST values (e.g., burned and secondary forests), rather than at the most
536 severely disturbed classes (e.g., crops and pastures, Figure 6). Among the forest classes,
537 variations in seasonal water stress manifested in ET-LST relationships in different ways: burned
538 and secondary forests showed little change from wet to dry season (differences in trend from -
539 0.04 to -0.02), whereas the dry season substantially improved ET-LST relationships at intact and
540 logged forests (differences in trend from 0.15 to 0.28; Figure 6, Table 2). These findings, along
541 with the ESI profile from Landsat (Figure 3B), suggest that patches of burned and secondary
542 forests, especially the most recent ones, experience year-round moisture stress (e.g., patches with
543 low ET and high LST even in the wet season). Therefore, strong inverse correlations between ET
544 and LST in wet periods could be used as an indicator of water stress and inform about the
545 functioning of disturbed forests.

546 Patchy mosaics are prominent following fires and can include severely disturbed patches
547 adjacent to fragments with substantial residual vegetation and organic matter (Chazdon, 2003).
548 In this sense, Landsat fine-scale ET and LST estimates showed improved discrimination of the
549 internal ET and LST variability of these patches. While MODIS data showed similarly low water
550 stress across all forest classes in January (Figure 3A), Landsat finer-scale data showed larger
551 differences among those classes even in the wet season (Figure 3B). These larger differences in
552 the Landsat-based ESI may imply that MODIS-based assessments of water fluxes or water-use
553 efficiency (e.g., Brunsell et al., 2020) are underestimating moisture deficit in these more
554 degraded and patchier areas such as burned forests.

555 Taken together, these results highlight the wide range of forest functional responses to
556 disturbances from a continuum of canopy structure and energy balance. This is a bi-directional
557 gradient, resulting from deforestation and degradation in one direction, and forest regeneration or
558 succession in the other. The characteristics of these disturbance gradients are integrally linked to
559 canopy structural properties and may influence energy balance components and associated
560 microclimates in linear or non-linear ways (Breshears, 2006; Stark et al., 2020). For example, as
561 woody plant cover decreases, albedo and near-ground solar radiation increase, which increases
562 the Bowen ratio (von Randow et al., 2004). Additionally, these patterns may also manifest
563 nonlinearly, displaying threshold-type responses. Near-ground solar radiation, for instance,
564 decreases nonlinearly with increasing canopy cover. Similarly, surface roughness and associated
565 wind flow category change nonlinearly with increasing cover (Breshears, 2006; Stark et al.,
566 2020).

567 **4.2. Forest structure controls on energy balance**

568 Although radiation controls on water and energy cycles prevail over our study area, forest
569 structure seems to be an important secondary control of transpiration in degraded and secondary
570 forests. Building on the Landsat-based ET and LST characterization during the dry season and
571 the structural characterization provided by GEDI data, we showed that forest structure
572 moderately explained ET and LST variability in the most heavily disturbed forests (burned and
573 secondary), whereas forest structure provided little or no ET and LST predictive power in the
574 least disturbed logged and intact forests (Figure 8). These findings suggest that disturbances
575 enhance ET biophysical controls (from forest structure) and that the contribution of canopy
576 structural properties to ET and LST is modulated by disturbances and the associated water stress.
577 Also, forest structure's contribution to ET decreased with time since disturbance, pointing to the
578 functional recovery of these forests, with decreasing water stress and biophysical control over
579 time as regeneration takes place.

580 Previous modelling studies converge with our findings. Using a land surface model, Mallick
581 et al. (2016) quantified the controls on evaporation and transpiration across representative plant
582 functional types in the Amazon and found enhanced biophysical influence on ET during the dry
583 season, especially over pastures and dry forest functional types. This same effect was observed
584 on the diurnal cycle, which shows higher VPD in the afternoon than in the morning, and during
585 the strong 2005 drought. Longo et al. (2020) investigated the effects of forest degradation on ET
586 using an ecosystem demography model, and found that the magnitude and seasonality of fluxes
587 were modulated by changes in forest structure caused by degradation. During the dry season and
588 under typical conditions, severely degraded forests (biomass loss $\geq 66\%$) experienced water

589 stress with declines in ET (up to 34%) and daily mean ground temperatures (up to 6.5°C) relative
590 to intact forests.

591 Studies using observational data such as satellite observations and flux tower measurements
592 also show degrees of agreement with our results. von Randow et al. (2012) found enhanced
593 biophysical control on ET for pastures during the dry season, whereas the findings from Oliveira
594 et al. (2019) suggested that the control of canopy stomatal conductance and root depth on
595 vegetation water use is stronger in agricultural systems than in primary and secondary forests in
596 the Amazon.

597 We observed larger ET and LST variability in the dry season for the majority of the forest
598 classes (Figure 5). Hasler and Avissar (2007) also found a larger scatter of ET values during dry
599 season throughout the Amazon and suggested that this effect is due to the increasing importance
600 of secondary drivers of latent heat flux in the dry period, such as VPD and water availability.
601 The ESI annual profile (Figure 3) showing increasing evaporative stress towards the end of the
602 dry season for all classes corroborates this. In contrast, the most recent classes (and likely, the
603 most impacted) of logged, burned and secondary forests showed larger ET variability in the wet
604 season (Figure 5), suggesting that these classes may be experiencing the dry season enhanced
605 biophysical controls during the wet season as well. This hypothesis is also supported by the
606 strong ET-LST relationships in these forests during both seasons (Figure 6).

607 Forest structure plays an essential role in determining roughness lengths and aerodynamic
608 conductance to heat, moisture, and momentum between the canopy and atmospheric (Bright et
609 al., 2015). Supporting the strong influence of forest structure on the canopy and aerodynamic
610 conductances, we found that ET and LST were strongly correlated with FHD, TCH, CC, and
611 PAI (Table 3). Moreover, the FHD metric (an indirect measure of surface roughness given by
612 structural complexity) was significantly lower in burned and secondary sites compared to intact
613 forests (Figure 7) likely leading to decreased canopy conductance to heat and moisture and
614 consequent lower ET and higher LST in these forests (Figure 5, Figure 6).

615 Due to their larger aerodynamic properties, forests are more efficient at dissipating sensible
616 heat away from the surface and into the boundary layer relative to areas with shorter vegetation,
617 particularly during the daytime (Bright et al., 2015; Hoffmann & Jackson, 2000). Our detailed
618 characterization of ET, LST and forest structure relationships strongly supports these statements,
619 as the classes with lower stature and complexity (described by CC and FHD metrics in Figure 7)
620 showed the highest temperatures on both wet and dry seasons (Figure 5). Moreover, the highest
621 correlation of the FHD metric with surface temperature also suggests that structural complexity
622 plays an important role in cooling the canopy.

623 4.3. Implications for vegetation modelling

624 Land cover changes (Davidson et al., 2012) and their positive feedbacks in the precipitation
625 variability in the Amazon Basin (Hilker et al., 2014; Wang et al., 2011) are expected to increase
626 the canopy–atmosphere coupling of forest systems under drier conditions by altering the ratio of
627 the biological and aerodynamic conductances. Our observational findings support previous
628 model-based and eddy-covariance findings showing that under drier conditions, the canopy-
629 atmosphere coupling increases, and so the biophysical controls on ET amplify as well. An
630 increase in biophysical control is an indicator of a potential transpiration shift from an energy-
631 limited to a water-limited regime (due to the impact of air and surface temperatures and VPD on
632 the canopy and aerodynamic conductance ratio), with further consequences for the global surface
633 water balance and rainfall recycling.

634 The implications of these findings to vegetation models in tropical forests are significant.
635 The largely aggregated ‘big-leaf’ vegetation models, which represent forests with single
636 functional types, may not be able to characterize complex and heterogeneous structure-climate
637 interactions across different forest types and disturbance conditions. Cohort-based vegetation
638 models (CBVM) stand between ‘big leaf’ and individual-based models and can efficiently
639 represent structural and functional diversity within forest ecosystems at regional and global
640 scales (Fisher et al., 2018). CBVM may provide a more appropriate way to account for forest
641 responses to the changes in the micro-environment caused by disturbances (Longo et al., 2020).
642 Explicitly incorporating forest structure information into CBVM to inform about the degradation
643 status and the degree of vegetation canopy coupling to the atmosphere could certainly improve
644 estimates of seasonal water and energy fluxes at heterogeneous forests such as those in the
645 Southern Amazon.

646 Acknowledgements

647 E. R. P. was supported by an Australian Government Research Training
648 Program Scholarship, and by the USDA Forest Service Pacific Northwest Research Station and
649 International Programs. The research carried out at the Jet Propulsion Laboratory, California
650 Institute of Technology, was under a contract with the National Aeronautics and Space
651 Administration. M. L. was supported by the NASA Postdoctoral Program, administered by
652 Universities Space Research Association under contract with NASA and the Next Generation
653 Ecosystem Experiments - Tropics, funded by the U.S. Department of Energy, Office of Science,
654 Office of Biological and Environmental Research.

655 Data Availability Statement

656 All remote sensing data utilized in this study is freely available for users. MODIS and GEDI
657 data can be accessed at the Land Processes Distributed Active Archive Center (LP DAAC -
658 <https://lpdaac.usgs.gov/>). Landsat ET and LST data can be accessed at the EEFLUX page
659 (<http://eeflux-level1.appspot.com/>).

660 References

- 661 Allen, R., Morton, C., Kamble, B., Kilic, A., Huntington, J., Thau, D., Gorelick, N., Erickson, T., Moore, R.,
662 Trezza, R., Ratcliffe, I., & Robison, C. (2015). EEFlux: A Landsat-based Evapotranspiration
663 mapping tool on the Google Earth Engine. 2015 ASABE / IA Irrigation Symposium: Emerging
664 Technologies for Sustainable Irrigation St. Joseph, MI.
- 665 Allen, R., Tasumi, M., & Trezza, R. (2007). Satellite-Based Energy Balance for Mapping
666 Evapotranspiration with Internalized Calibration (METRIC) - Model. *Journal of Irrigation and*
667 *Drainage Engineering*, 133(4), 380-394. [https://doi.org/doi:10.1061/\(ASCE\)0733-
668 9437\(2007\)133:4\(395\)](https://doi.org/doi:10.1061/(ASCE)0733-9437(2007)133:4(395))
- 669 Almeida, C. A. D., Coutinho, A. C., Esquerdo, J. C. D. M., Adami, M., Venturieri, A., Diniz, C. G., Dessay, N.,
670 Durieux, L., & Gomes, A. R. (2016). High spatial resolution land use and land cover mapping of
671 the Brazilian Legal Amazon in 2008 using Landsat-5/TM and MODIS data. *Acta Amazonica*, 46(3),
672 291-302. <https://doi.org/10.1590/1809-4392201505504>
- 673 Anderson, M. C., Allen, R. G., Morse, A., & Kustas, W. P. (2012). Use of Landsat thermal imagery in
674 monitoring evapotranspiration and managing water resources. *Remote Sensing of Environment*,
675 122, 50-65.
- 676 Arvor, D., Dubreuil, V., Ronchail, J., Simões, M., & Funatsu, B. M. (2014). Spatial patterns of rainfall
677 regimes related to levels of double cropping agriculture systems in Mato Grosso (Brazil).
678 *International Journal of Climatology*, 34(8), 2622-2633.
679 <https://doi.org/https://doi.org/10.1002/joc.3863>
- 680 Barkhordarian, A., Saatchi, S. S., Behrangi, A., Loikith, P. C., & Mechoso, C. R. (2019). A Recent
681 Systematic Increase in Vapor Pressure Deficit over Tropical South America. *Scientific Reports*,
682 9(1), 15331. <https://doi.org/10.1038/s41598-019-51857-8>
- 683 Bastiaanssen, W. G. M., Menenti, M., Feddes, R. A., & Holtslag, A. A. M. (1998). A remote sensing
684 surface energy balance algorithm for land (SEBAL). 1. Formulation. *Journal of Hydrology*, 212-
685 213, 198-212. [https://doi.org/https://doi.org/10.1016/S0022-1694\(98\)00253-4](https://doi.org/https://doi.org/10.1016/S0022-1694(98)00253-4)
- 686 Bonan, G. B. (2008). Forests and Climate Change: Forcings, Feedbacks, and the Climate Benefits of
687 Forests. *Science*, 320(5882), 1444-1449. <https://doi.org/10.1126/science.1155121>
- 688 Brando, P. M., Silvério, D., Maracahipes-Santos, L., Oliveira-Santos, C., Levick, S. R., Coe, M. T.,
689 Migliavacca, M., Balch, J. K., Macedo, M. N., Nepstad, D. C., Maracahipes, L., Davidson, E., Asner,
690 G., Kolle, O., & Trumbore, S. (2019). Prolonged tropical forest degradation due to compounding
691 disturbances: Implications for CO₂ and H₂O fluxes. *Global Change Biology*, 25(9), 2855-2868.
692 <https://doi.org/10.1111/gcb.14659>
- 693 Breshears, D. D. (2006). The grassland–forest continuum: trends in ecosystem properties for woody
694 plant mosaics? [[https://doi.org/10.1890/1540-9295\(2006\)0040096:TGCTIE.2.0.CO;2](https://doi.org/10.1890/1540-9295(2006)0040096:TGCTIE.2.0.CO;2)]. *Frontiers*
695 *in Ecology and the Environment*, 4(2), 96-104. [https://doi.org/https://doi.org/10.1890/1540-
696 9295\(2006\)004\[0096:TGCTIE\]2.0.CO;2](https://doi.org/https://doi.org/10.1890/1540-9295(2006)004[0096:TGCTIE]2.0.CO;2)
- 697 Bright, R. M., Zhao, K., Jackson, R. B., & Cherubini, F. (2015). Quantifying surface albedo and other direct
698 biogeophysical climate forcings of forestry activities. *Global Change Biology*, 21(9), 3246-3266.
699 <https://doi.org/https://doi.org/10.1111/gcb.12951>
- 700 Brunsell, N. A., De Oliveira, G., Barlage, M., Shimabukuro, Y., Moraes, E., & Aragão, L. (2020).
701 Examination of seasonal water and carbon dynamics in eastern Amazonia: a comparison of
702 Noah-MP and MODIS. *Theoretical and Applied Climatology*. [https://doi.org/10.1007/s00704-
703 020-03435-6](https://doi.org/10.1007/s00704-020-03435-6)

- 704 Chazdon, R. L. (2003). Tropical forest recovery: legacies of human impact and natural disturbances.
 705 *Perspectives in Plant Ecology, Evolution and Systematics*, 6(1), 51-71.
 706 <https://doi.org/https://doi.org/10.1078/1433-8319-00042>
- 707 Coe, M., Macedo, M., Brando, P., Lefebvre, P., Panday, P., & Silv rio, D. (2016). The Hydrology and
 708 Energy Balance of the Amazon Basin. In (Vol. 227, pp. 35-53). [https://doi.org/10.1007/978-3-](https://doi.org/10.1007/978-3-662-49902-3_3)
 709 [662-49902-3_3](https://doi.org/10.1007/978-3-662-49902-3_3)
- 710 Costa, M. H., & Foley, J. A. (1997). Water balance of the Amazon Basin: Dependence on vegetation cover
 711 and canopy conductance. *Journal of Geophysical Research: Atmospheres*, 102(D20), 23973-
 712 23989.
- 713 da Rocha, H. R., Manzi, A. O., Cabral, O. M., Miller, S. D., Goulden, M. L., Saleska, S. R., R-Coupe, N.,
 714 Wofsy, S. C., Borma, L. S., Artaxo, P., Vourlitis, G., Nogueira, J. S., Cardoso, F. L., Nobre, A. D.,
 715 Kruijt, B., Freitas, H. C., von Randow, C., Aguiar, R. G., & Maia, J. F. (2009). Patterns of water and
 716 heat flux across a biome gradient from tropical forest to savanna in Brazil. *Journal of*
 717 *Geophysical Research: Biogeosciences*, 114(G1).
 718 <https://doi.org/https://doi.org/10.1029/2007JG000640>
- 719 Da Silva, P. E., Santos e Silva, C. M., Spyrides, M. H. C., & Andrade, L. d. M. B. (2019). Precipitation and
 720 air temperature extremes in the Amazon and northeast Brazil. *International Journal of*
 721 *Climatology*, 39(2), 579-595. <https://doi.org/https://doi.org/10.1002/joc.5829>
- 722 Davidson, E. A., de Araujo, A. C., Artaxo, P., Balch, J. K., Brown, I. F., Bustamante, M. M., Coe, M. T.,
 723 DeFries, R. S., Keller, M., & Longo, M. (2012). The Amazon basin in transition. *Nature*, 481(7381),
 724 321-328.
- 725 Diniz, C. G., Souza, A. A. d. A., Santos, D. C., Dias, M. C., Luz, N. C. d., Moraes, D. R. V. d., Maia, J. S.,
 726 Gomes, A. R., Narvaes, I. d. S., Valeriano, D. M., Maurano, L. E. P., & Adami, M. (2015). DETER-B:
 727 The New Amazon Near Real-Time Deforestation Detection System. *IEEE Journal of Selected*
 728 *Topics in Applied Earth Observations and Remote Sensing*, 8(7), 3619-3628.
 729 <https://doi.org/10.1109/JSTARS.2015.2437075>
- 730 Dubayah, R., Armston, J., Healey, S. P., Bruening, J. M., Patterson, P. L., Kellner, J. R., Duncanson, L.,
 731 Saarela, S., St hl, G., Yang, Z., Tang, H., Blair, J. B., Fatoyinbo, L., Goetz, S., Hancock, S., Hansen,
 732 M., Hofton, M., Hurtt, G., & Luthcke, S. (2022). GEDI launches a new era of biomass inference
 733 from space. *Environmental Research Letters*, 17(9), 095001. [https://doi.org/10.1088/1748-](https://doi.org/10.1088/1748-9326/ac8694)
 734 [9326/ac8694](https://doi.org/10.1088/1748-9326/ac8694)
- 735 Dubayah, R., Blair, J. B., Goetz, S., Fatoyinbo, L., Hansen, M., Healey, S., Hofton, M., Hurtt, G., Kellner, J.,
 736 Luthcke, S., Armston, J., Tang, H., Duncanson, L., Hancock, S., Jantz, P., Marselis, S., Patterson, P.
 737 L., Qi, W., & Silva, C. (2020). The Global Ecosystem Dynamics Investigation: High-resolution laser
 738 ranging of the Earth's forests and topography. *Science of Remote Sensing*, 1, 100002.
 739 <https://doi.org/https://doi.org/10.1016/j.srs.2020.100002>
- 740 Duncanson, L., Kellner, J. R., Armston, J., Dubayah, R., Minor, D. M., Hancock, S., Healey, S. P., Patterson,
 741 P. L., Saarela, S., Marselis, S., Silva, C. E., Bruening, J., Goetz, S. J., Tang, H., Hofton, M., Blair, B.,
 742 Luthcke, S., Fatoyinbo, L., Abernethy, K., . . . Zraggen, C. (2022). Aboveground biomass density
 743 models for NASA's Global Ecosystem Dynamics Investigation (GEDI) lidar mission. *Remote*
 744 *Sensing of Environment*, 270, 112845.
 745 <https://doi.org/https://doi.org/10.1016/j.rse.2021.112845>
- 746 Fisher, J. B. (2013). Land-Atmosphere Interactions, Evapotranspiration. In E. G. Njoku (Ed.), *Encyclopedia*
 747 *of Remote Sensing* (pp. 1-5). Springer-Verlag.
- 748 Fisher, J. B., Malhi, Y., Bonal, D., da Rocha, H. R., C. de Araujo, A., Gamo, M., Goulden, M. L., Hirano, T.,
 749 Huete, A., Kondo, H., Kumagai, T. O., Loeschner, H. W., Miller, S. D., Nobre, A., Nouvellon, Y.,
 750 Oberbauer, S. F., Panuthai, S., Rouspard, O., Saleska, S., . . . Von Randow, C. (2009). The land-
 751 atmosphere water flux in the tropics. *Global Change Biology*, 15(11), 2694-2714.
 752 <https://doi.org/10.1111/j.1365-2486.2008.01813.x>
- 753 Fisher, J. B., Melton, F., Middleton, E., Hain, C., Anderson, M., Allen, R., McCabe, M. F., Hook, S.,
 754 Baldocchi, D., Townsend, P. A., Kilic, A., Tu, K., Miralles, D. D., Perret, J., Lagouarde, J.-P.,
 755 Waliser, D., Purdy, A. J., French, A., Schimel, D., . . . Wood, E. F. (2017). The future of
 756 evapotranspiration: Global requirements for ecosystem functioning, carbon and climate

757 feedbacks, agricultural management, and water resources. *Water Resources Research*, 53(4),
758 2618-2626. <https://doi.org/10.1002/2016wr020175>

759 Fisher, J. B., Tu, K. P., & Baldocchi, D. D. (2008). Global estimates of the land-atmosphere water flux
760 based on monthly AVHRR and ISLSCP-II data, validated at 16 FLUXNET sites. *Remote Sensing of*
761 *Environment*, 112(3), 901-919. <https://doi.org/https://doi.org/10.1016/j.rse.2007.06.025>

762 Fisher, R. A., Koven, C. D., Anderegg, W. R. L., Christoffersen, B. O., Dietze, M. C., Farris, C. E., Holm, J.
763 A., Hurtt, G. C., Knox, R. G., Lawrence, P. J., Lichstein, J. W., Longo, M., Matheny, A. M., Medvigy,
764 D., Muller-Landau, H. C., Powell, T. L., Serbin, S. P., Sato, H., Shuman, J. K., . . . Moorcroft, P. R.
765 (2018). Vegetation demographics in Earth System Models: A review of progress and priorities.
766 *Global Change Biology*, 24(1), 35-54. <https://doi.org/https://doi.org/10.1111/gcb.13910>

767 Hasler, N., & Avissar, R. (2007). What Controls Evapotranspiration in the Amazon Basin? *Journal of*
768 *Hydrometeorology*, 8(3), 380-395. <https://doi.org/10.1175/jhm587.1>

769 Hilker, T., Lyapustin, A. I., Tucker, C. J., Hall, F. G., Myneni, R. B., Wang, Y., Bi, J., de Moura, Y. M., &
770 Sellers, P. J. (2014). Vegetation dynamics and rainfall sensitivity of the Amazon. *Proceedings of*
771 *the National Academy of Sciences*, 111(45), 16041-16046.

772 Hoffmann, W. A., & Jackson, R. B. (2000). Vegetation-Climature Feedbacks in the Conversion of Tropical
773 Savanna to Grassland. *Journal of Climate*, 13(9), 1593-1602. [https://doi.org/10.1175/1520-0442\(2000\)013<1593:Vcfitc>2.0.Co;2](https://doi.org/10.1175/1520-0442(2000)013<1593:Vcfitc>2.0.Co;2)

774 Hofton, M., Blair, J. B., Story, S., & Yi, D. (2019). Algorithm Theoretical Basis Document (ATBD) for
775 GEDI Transmit and Receive Waveform Processing for L1 and L2 Products. V. 1.0.

776 Huang, M., Xu, Y., Longo, M., Keller, M., Knox, R. G., Koven, C. D., & Fisher, R. A. (2020). Assessing
777 impacts of selective logging on water, energy, and carbon budgets and ecosystem dynamics in
778 Amazon forests using the Functionally Assembled Terrestrial Ecosystem Simulator.
779 *Biogeosciences*, 17(20), 4999-5023. <https://doi.org/10.5194/bg-17-4999-2020>

780 IBGE. (2021). *Mapeamento de Recursos Naturais do Brasil - Escala 1:250.000 - Versão 2021* Version
781 2021). <https://www.ibge.gov.br/geociencias/informacoes-ambientais/vegetacao/22453-cartas-1-250-000.html?=&t=downloads>

782
783

784 INPE. (2020). PRODES - Monitoramento da Floresta Amazônica por Satélite. In São José dos Campos,
785 Brazil: National Institute for Space Research.

786 Jarvis, P. G., & McNaughton, K. G. (1986). Stomatal Control of Transpiration: Scaling Up from Leaf to
787 Region. In A. MacFadyen & E. D. Ford (Eds.), *Advances in Ecological Research* (Vol. 15, pp. 1-49).
788 Academic Press. [https://doi.org/https://doi.org/10.1016/S0065-2504\(08\)60119-1](https://doi.org/https://doi.org/10.1016/S0065-2504(08)60119-1)

789 Jucker, T., Hardwick, S. R., Both, S., Elias, D. M. O., Ewers, R. M., Milodowski, D. T., Swinfield, T., &
790 Coomes, D. A. (2018). Canopy structure and topography jointly constrain the microclimate of
791 human-modified tropical landscapes. *Global Change Biology*, 24(11), 5243-5258.
792 <https://doi.org/https://doi.org/10.1111/gcb.14415>

793 Lathuillière, M. J., Johnson, M. S., & Donner, S. D. (2012). Water use by terrestrial ecosystems: temporal
794 variability in rainforest and agricultural contributions to evapotranspiration in Mato Grosso,
795 Brazil. *Environmental Research Letters*, 7(2), 024024.

796 Lefsky, M., Cohen, W. B., Parker, G., & Harding, D. J. (2002). Lidar Remote Sensing for Ecosystem
797 Studies. *BioScience*, 52(1), 19-30.

798 Longo, M., Saatchi, S., Keller, M., Bowman, K., Ferraz, A., Moorcroft, P. R., Morton, D. C., Bonal, D.,
799 Brando, P., Burban, B., Derroire, G., dos-Santos, M. N., Meyer, V., Saleska, S., Trumbore, S., &
800 Vincent, G. (2020). Impacts of Degradation on Water, Energy, and Carbon Cycling of the Amazon
801 Tropical Forests. *Journal of Geophysical Research: Biogeosciences*, 125(8), e2020JG005677.
802 <https://doi.org/https://doi.org/10.1029/2020JG005677>

803 Maeda, E., Ma, X., Wagner, F., Kim, H., Oki, T., Eamus, D., & Huete, A. (2017). Evapotranspiration
804 seasonality across the Amazon Basin. *Earth System Dynamics*, 8, 439-454.
805 <https://doi.org/10.5194/esd-8-439-2017>

806 Malhi, Y., Pegoraro, E., Nobre, A. D., Pereira, M. G., Grace, J., Culf, A. D., & Clement, R. (2002). Energy
807 and water dynamics of a central Amazonian rain forest. *Journal of Geophysical Research:*
808 *Atmospheres*, 107(D20), LBA 45-41-LBA 45-17.

809 Mallick, K., Trebs, I., Boegh, E., Giustarini, L., Schlerf, M., Drewry, D., Hoffmann, L., Von Randow, C.,
810 Kruijt, B., Araújo, A., Saleska, S., Ehleringer, J. R., Domingues, T. F., Ometto, J. P. H. B., Nobre, A.
811 D., De Moraes, O. L. L., Hayek, M., Munger, J. W., & Wofsy, S. (2016). *Canopy-scale biophysical*
812 *controls of transpiration and evaporation in the Amazon Basin*. Copernicus GmbH.
813 <https://dx.doi.org/10.5194/hess-2015-552>

814 MapBiomas Project. (2019, 2019). *The Brazilian Annual Land Use and Land Cover Mapping Project –*
815 *Collection 4.0* Retrieved September 12 2019 from <https://mapbiomas.org/en>

816 Matricardi, E. A., Skole, D. L., Pedlowski, M. A., Chomentowski, W., & Fernandes, L. C. (2010).
817 Assessment of tropical forest degradation by selective logging and fire using Landsat imagery.
818 *Remote Sensing of Environment*, 114(5), 1117-1129.

819 Miller, S. D., Goulden, M. L., Hutrya, L. R., Keller, M., Saleska, S. R., Wofsy, S. C., Figueira, A. M. S., Da
820 Rocha, H. R., & De Camargo, P. B. (2011). Reduced impact logging minimally alters tropical
821 rainforest carbon and energy exchange. *Proceedings of the National Academy of Sciences*,
822 108(48), 19431-19435. <https://doi.org/10.1073/pnas.1105068108>

823 Monteith, J. (1965). The state and movement of water in living organisms. 19th Symposia of the Society
824 for Experimental Biology. Cambridge University Press, London, 1965,

825 Morton, D., Le Page, Y., DeFries, R., Collatz, G., & Hurtt, G. (2013). Understorey fire frequency and the
826 fate of burned forests in southern Amazonia. *Philosophical Transactions of the Royal Society B:*
827 *Biological Sciences*, 368(1619), 20120163.

828 Mu, Q., Zhao, M., & Running, S. W. (2011). Improvements to a MODIS global terrestrial
829 evapotranspiration algorithm. *Remote Sensing of Environment*, 115(8), 1781-1800.
830 <https://doi.org/https://doi.org/10.1016/j.rse.2011.02.019>

831 Nepstad, D. C., de Carvalho, C. R., Davidson, E. A., Jipp, P. H., Lefebvre, P. A., Negreiros, G. H., da Silva, E.
832 D., Stone, T. A., Trumbore, S. E., & Vieira, S. (1994). The role of deep roots in the hydrological
833 and carbon cycles of Amazonian forests and pastures. *Nature*, 372(6507), 666-669.
834 <https://doi.org/10.1038/372666a0>

835 Numata, I., Khand, K., Kjaersgaard, J., Cochrane, M. A., & Silva, S. S. (2017). Evaluation of Landsat-Based
836 METRIC Modeling to Provide High-Spatial Resolution Evapotranspiration Estimates for
837 Amazonian Forests. *Remote Sensing*, 9(1), 46. <https://www.mdpi.com/2072-4292/9/1/46>

838 O'Connor, J., Santos, M. J., Rebel, K. T., & Dekker, S. C. (2019). The influence of water table depth on
839 evapotranspiration in the Amazon arc of deforestation. *Hydrol. Earth Syst. Sci.*, 23(9), 3917-
840 3931. <https://doi.org/10.5194/hess-23-3917-2019>

841 Oliveira, G., Brunsell, N. A., Moraes, E. C., Shimabukuro, Y. E., Santos, T. V., Randow, C., Aguiar, R. G., &
842 Aragao, L. E. O. C. (2019). Effects of land-cover changes on the partitioning of surface energy
843 and water fluxes in Amazonia using high-resolution satellite imagery. *Ecohydrology*, 12(6),
844 e2126. <https://doi.org/10.1002/eco.2126>

845 R Core Team. (2021). *R: A Language and Environment for Statistical Computing*. In R Foundation for
846 Statistical Computing. <https://www.R-project.org/>

847 Rangel Pinagé, E., M. Bell, D., Longo, M., Gao, S., Keller, M., Silva, C. A., Ometto, J. P., Köhler, P.,
848 Frankenberg, C., & Huete, A. (2022). Forest structure and solar-induced fluorescence across
849 intact and degraded forests in the Amazon. *Remote Sensing of Environment*, 274, 112998.
850 <https://doi.org/https://doi.org/10.1016/j.rse.2022.112998>

851 Restrepo-Coupe, N., da Rocha, H. R., Hutrya, L. R., da Araujo, A. C., Borma, L. S., Christoffersen, B.,
852 Cabral, O. M., de Camargo, P. B., Cardoso, F. L., & da Costa, A. C. L. (2013). What drives the
853 seasonality of photosynthesis across the Amazon basin? A cross-site analysis of eddy flux tower
854 measurements from the Brasil flux network. *Agricultural and forest meteorology*, 182, 128-144.

855 Running, S. W., Mu, Q., & Zhao, M. (2017). *MYD16A2 MODIS/Aqua Net Evapotranspiration 8-Day L4*
856 *Global 500m SIN Grid V006*. <https://doi.org/https://doi.org/10.5067/MODIS/MYD16A2.006>.

857 Silva, C. A., Hamamura, C., Valbuena, R., Hancock, S., Cardil, A., Broadbent, E. N., Almeida, D. R. A. d.,
858 Junior, C. H. L. S., & Klauber, C. (2020). rGEDI: NASA's Global Ecosystem Dynamics Investigation
859 (GEDI) Data Visualization and Processing. *R package version 0.1.7* [https://CRAN.R-](https://CRAN.R-project.org/package=rGEDI)
860 [project.org/package=rGEDI](https://CRAN.R-project.org/package=rGEDI)

861 Silvério, D. V., Brando, P. M., Macedo, M. N., Beck, P. S. A., Bustamante, M., & Coe, M. T. (2015).
862 Agricultural expansion dominates climate changes in southeastern Amazonia: the overlooked

863 non-GHG forcing. *Environmental Research Letters*, 10(10), 104015.
864 <https://doi.org/10.1088/1748-9326/10/10/104015>

865 Souza, C. M., Roberts, D. A., & Cochrane, M. A. (2005). Combining spectral and spatial information to
866 map canopy damage from selective logging and forest fires. *Remote Sensing of Environment*,
867 98(2), 329-343. <https://doi.org/https://doi.org/10.1016/j.rse.2005.07.013>

868 Spracklen, D. V., Arnold, S. R., & Taylor, C. M. (2012). Observations of increased tropical rainfall
869 preceded by air passage over forests. *Nature*, 489(7415), 282-285.
870 <https://doi.org/10.1038/nature11390>

871 Spracklen, D. V., Baker, J. C. A., Garcia-Carreras, L., & Marsham, J. H. (2018). The Effects of Tropical
872 Vegetation on Rainfall. *Annual Review of Environment and Resources*, 43(1), 193-218.
873 <https://doi.org/10.1146/annurev-environ-102017-030136>

874 Stark, S. C., Breshears, D. D., Aragón, S., Villegas, J. C., Law, D. J., Smith, M. N., Minor, D. M., de Assis, R.
875 L., de Almeida, D. R. A., de Oliveira, G., Saleska, S. R., Swann, A. L. S., Moura, J. M. S., Camargo, J.
876 L., da Silva, R., Aragão, L. E. O. C., & Oliveira, R. C. (2020). Reframing tropical savannization:
877 linking changes in canopy structure to energy balance alterations that impact climate.
878 *Ecosphere*, 11(9), e03231. <https://doi.org/https://doi.org/10.1002/ecs2.3231>

879 Tang, H., & Armston, J. (2019). *Algorithm Theoretical Basis Document (ATBD) for GEDI L2B Footprint*
880 *Canopy Cover and Vertical Profile Metrics* Retrieved July 29th from
881 https://lpdaac.usgs.gov/documents/588/GEDI_FCCVPM_ATBD_v1.0.pdf

882 Tukey, J. W. (1977). *Exploratory data analysis* (Vol. 2). Reading, MA.

883 van der Ent, R. J., Savenije, H. H. G., Schaeffli, B., & Steele-Dunne, S. C. (2010). Origin and fate of
884 atmospheric moisture over continents. *Water Resources Research*, 46(9).
885 <https://doi.org/10.1029/2010wr009127>

886 von Randow, C., Manzi, A. O., Kruijt, B., de Oliveira, P. J., Zanchi, F. B., Silva, R. L., Hodnett, M. G., Gash, J.
887 H. C., Elbers, J. A., Waterloo, M. J., Cardoso, F. L., & Kabat, P. (2004). Comparative
888 measurements and seasonal variations in energy and carbon exchange over forest and pasture
889 in South West Amazonia. *Theoretical and Applied Climatology*, 78(1), 5-26.
890 <https://doi.org/10.1007/s00704-004-0041-z>

891 von Randow, R. C. S., von Randow, C., Hutjes, R. W. A., Tomasella, J., & Kruijt, B. (2012).
892 Evapotranspiration of deforested areas in central and southwestern Amazonia. *Theoretical and*
893 *Applied Climatology*, 109(1), 205-220. <https://doi.org/10.1007/s00704-011-0570-1>

894 Von Randow, R. D. C. S., Tomasella, J., Von Randow, C., De Araújo, A. C., Manzi, A. O., Hutjes, R., & Kruijt,
895 B. (2020). Evapotranspiration and gross primary productivity of secondary vegetation in
896 Amazonia inferred by eddy covariance. *Agricultural and forest meteorology*, 294, 108141.
897 <https://doi.org/10.1016/j.agrformet.2020.108141>

898 Vourlitis, G. L., de Souza Nogueira, J., de Almeida Lobo, F., Sendall, K. M., de Paulo, S. R., Antunes Dias,
899 C. A., Pinto Jr., O. B., & de Andrade, N. L. R. (2008). Energy balance and canopy conductance of a
900 tropical semi-deciduous forest of the southern Amazon Basin. *Water Resources Research*, 44(3).
901 <https://doi.org/https://doi.org/10.1029/2006WR005526>

902 Wang, G., Sun, S., & Mei, R. (2011). Vegetation dynamics contributes to the multi-decadal variability of
903 precipitation in the Amazon region. *Geophysical Research Letters*, 38(19).
904 <https://doi.org/https://doi.org/10.1029/2011GL049017>

905 Wulder, M. A., Loveland, T. R., Roy, D. P., Crawford, C. J., Masek, J. G., Woodcock, C. E., Allen, R. G.,
906 Anderson, M. C., Belward, A. S., Cohen, W. B., Dwyer, J., Erb, A., Gao, F., Griffiths, P., Helder, D.,
907 Herosilla, T., Hipple, J. D., Hostert, P., Hughes, M. J., . . . Zhu, Z. (2019). Current status of
908 Landsat program, science, and applications. *Remote Sensing of Environment*, 225, 127-147.
909 <https://doi.org/https://doi.org/10.1016/j.rse.2019.02.015>

910 Zemp, D. C., Schleussner, C.-F., Barbosa, H. M. J., Hirota, M., Montade, V., Sampaio, G., Staal, A., Wang-
911 Erlandsson, L., & Rammig, A. (2017). Self-amplified Amazon forest loss due to vegetation-
912 atmosphere feedbacks [Article]. *Nature Communications*, 8, 14681.
913 <https://doi.org/10.1038/ncomms14681>

914 <http://www.nature.com/articles/ncomms14681#supplementary-information>

915

